Seismic Performance of Embedded Column Base Connections with Attached Reinforcement: Tests and Strength Models

Ahmad S. Hassan and Amit M. Kanvinde

ABSTRACT

Embedded column base (ECB) connections used in mid- to high-rise steel moment frames derive moment resistance through bearing of the embedded column and base plate against the concrete footing. Five large-scale tests on ECB connections are presented; these feature cantilever columns subjected to axial compression and cyclic lateral loading. The tests feature reinforcement details including (1) horizontal reinforcement bars attached to the column (either directly welded to the flanges or in the form of U-hairpins wrapped around the column), and (2) vertical reinforcement in the form of stirrups in the footing. These tests complement previous experiments that are nominally identical but without the additional reinforcement. The tests indicate that while the horizontal reinforcement enhances moment strength due to resisting forces in the horizontal direction, it also produces a tension field that decreases the restraint to the rotation of the embedded base plate, ultimately reducing overall moment strength. The addition of vertical reinforcement in the form of stirrups mitigates this issue to an extent. A strength model considering these effects is proposed and shown to predict strength with good accuracy across a range of configurations, encompassing the different configurations of horizontal and vertical reinforcement. Limitations of the approach are discussed.

Keywords: base connection, moment frames, composite connection.

INTRODUCTION

Embedded column base (ECB) connections in seismically designed steel moment frames (SMFs) are commonly used to connect the steel columns to concrete foundations for mid- to high-rise buildings. Unlike low-rise buildings for which exposed-type base plate connections [where a base plate is welded to the column with anchor rods attached to the foundation, see Figure 1(a)] are suitable, in mid- to high-rise frames, the embedment is required to resist large base moments and provide fixity through bearing of column flanges against concrete, as shown in Figure 1(b). The column is usually welded to a base plate resting on a thin concrete layer for leveling purposes. Face-bearing plates are often used on the top of concrete surface to transfer axial compression and facilitate the formation of a shear panel similar to composite beam-column connections (ASCE, 1994).

Significant research has been conducted on exposed-type base connections, including large-scale experimental testing (Astaneh et al., 1992; Fahmy et al., 1999; Gomez et al., 2010; Kanvinde et al., 2015; Trautner et al., 2017; and Hassan et al., 2022), analytical (Wald, 2000), and computational simulations for both component (Inamasu et al., 2021; Hassan et al., 2022), and frame (Falborski et al., 2020), leading to the development of design considerations (Fisher and Kloiber, 2006; AISC, 2016; SEAOC, 2015). In contrast, research on ECB connections is sparse, with no experimentally validated strength characterization methods for design, and only limited finite element parametric studies (Pertold et al., 2000a, 2000b). Current design practice in the United States relies on adaptations of methods developed for other similar components such as composite beam-column connections (ASCE, 1994) and steel coupling beams embedded in concrete shear walls (Marcakis and Mitchell, 1980; Mattock and Gaafar, 1982; Harris et al., 1993; Shahrooz et al., 1993). The AISC *Seismic Design Manual* (AISC, 2018) applies the method developed by Mattock and Gaafar (1982) for coupling beams to the design of ECB connections. These adaptations disregard or inadequately incorporate behavioral aspects specific to ECB connections including (1) the effect of concrete confinement, which is limited in a shear wall or a composite beam-column connection; (2) the presence of a base plate welded to the column section; (3) the presence of axial load; and (4) differences in reinforcing bar patterns. Other studies on similar connections (Cui et al., 2009; Richards et al., 2018; Hanks and Richards, 2019) examined the effect of an overtopping slab-on-grade on top of an exposed-type column base connection. This type of connection (known as a blockout column base connection) is distinct from an

Ahmad S. Hassan, Designer, Degenkolb Engineers, Sacramento, Calif. Email: ahassan@degenkolb.com (Corresponding author)

Amit M. Kanvinde, Professor, Department of Civil and Environmental Engineering, University of California, Davis, Calif. Email: kanvinde@ucdavis.edu

Paper No. 2023-03

ECB connection in fundamental behavioral characteristics, wherein the concrete embedment due to the floor slab is incidental and the primary mode of moment resistance is similar to exposed-type base plate connections. As a consequence, behavioral characteristics of these connections are not readily applicable to ECB connections.

Previous experimental studies (Grilli et al., 2017) on ECB connections representative of U.S. construction practice—similar to that shown in Figure 1(b)—serve as the only test data available on the seismic performance of such connections. These five specimens featured wide-flange steel cantilever columns embedded within a concrete footing subjected to a cyclic lateral deformation history under a constant axial force (compression or tension). The specimens were designed with minimal longitudinal and transverse reinforcement such that observed failure modes and strengths were mainly associated with the concrete.

The results from this experimental program (Grilli et al., 2017; Grilli and Kanvinde, 2017), provided insights into the fundamental physics of the ECB connections, including failure modes that informed the development of strength models suitable for the design of ECB connections. Figure 1(b) shows the two primary mechanisms of moment resistance, as outlined by Grilli and Kanvinde (2017): (1) horizontal bearing stresses against the column flanges along with a complementary shear panel zone and (2) vertical bearing stresses resisting uplift of the base plate. Figures 2(a) and (b) show post-test photographs illustrating the failure modes observed from two specimens in the experimental program (Grilli et al., 2017) with different embedment depths. In

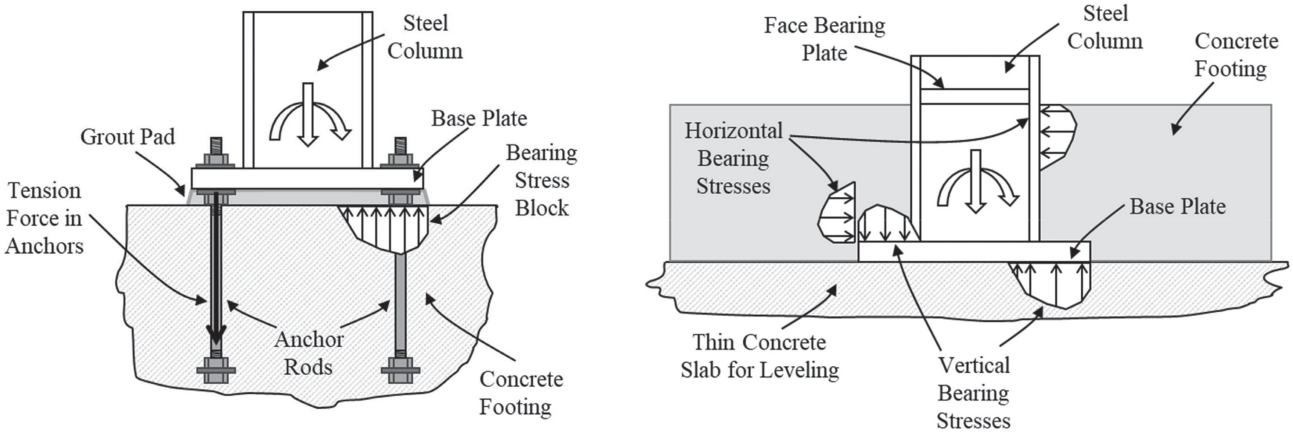

(a) Exposed-type connection *(b) Embedded-type (ECB) connection*

Fig. 1. Column base connections and force transfer mechanisms.

(a) Horizontal bearing *(b) Vertical bearing*

Fig. 2. Experimental program (Grilli et al., 2017) damage patterns suggesting modes of failure/deformation governed by bearing mechanisms.

summary, the singular study on ECB connections is limited by a relatively small data set and the examination of a single detail. Specifically, the test series included only one generic detail [similar to Figure 1(b)] without any reinforcement attached to the column. As a result, the test data do not represent the effect of such reinforcement that is commonly used in practice.

Motivated by these issues, this paper presents a series of five large-scale experiments on ECB connections with attached reinforcement bars, representative of construction practice in the United States, along with a strength model. Figure 3 schematically illustrates the main features of the tested details developed in consultation with an oversight committee of practitioners and fabricators (see the Acknowledgments section). These details are similar to the one examined by Grilli et al. (2017), with the exception of reinforcement fixtures attached to the embedded column flanges. Two techniques for reinforcement attachment are examined—welded reinforcement bars to the column flange (deformed weldable bars commonly used in practice), as shown in Figure 3(a), and "U-bar hairpin" reinforcement bars (recommended by the AISC *Seismic Provisions* for steel coupling beams) anchored by the embedded portion of the column and alternating in direction to engage both column flanges, as shown in Figure 3(b).

CURRENT PRACTICE AND AVAILABLE STRENGTH MODELS

The AISC *Seismic Provisions* (AISC, 2016) and Design Guide 1 (Fisher and Kloiber, 2006) illustrate embedded base connections but do not provide or recommend strength models or design approaches. The only such guidance is available in the AISC *Seismic Design Manual* (AISC, 2018). Figure 4(a) illustrates the assumptions adopted by this approach, referred to hereafter as the AISC SDM Method. Referring to this figure, the applied moment and shear are resisted through the development of bearing stress blocks on both sides of the embedded column flanges. Equation 1 provides a closed-form solution for the moment capacity, obtained by solving for the force and moment equilibrium based on the assumed stress blocks. This equation is based on the work done by Mattock and Gafaar (1982) for steel coupling beams embedded in concrete shear walls:

$$M_{base}^{AISC\ SDM} = 1.54\sqrt{f_c'}\left(\frac{b_w}{b_f}\right)^{0.66}\beta_1 b_f L_e \frac{g}{2}\left(\frac{0.58-0.22\beta_1}{0.88+\frac{g}{2L_e}}\right) \quad (1)$$

where

L_e = embedment depth of the steel column measured from the face of the foundation [as shown in Figure 4(a)]

b_f = width of the embedded section (column) flange, in.

b_w = width of concrete foundation perpendicular to the loading direction (b_w is the thickness of the wall pier in the original equation), in.

f_c' = specified compressive strength of concrete, ksi

$\frac{g}{2}$ = distance from the top surface of the foundation to the inflection point of the column, in.

β_1 = factor relating the depth of the equivalent rectangular stress block to the neutral axis depth, c, as defined in ACI 318-19 (ACI, 2019)

The term $\left(\frac{b_w}{b_f}\right)^{0.66}$ accounts for the effect of concrete confinement and the spread of compressive stress ahead of the column flange, such that the value 0.66 is calibrated to match experimental results by Mattock and Gaafar.

Referring to Figure 4(a), the values c/L_e and k_2 are assumed to be 0.66 and 0.36, respectively, as reported by

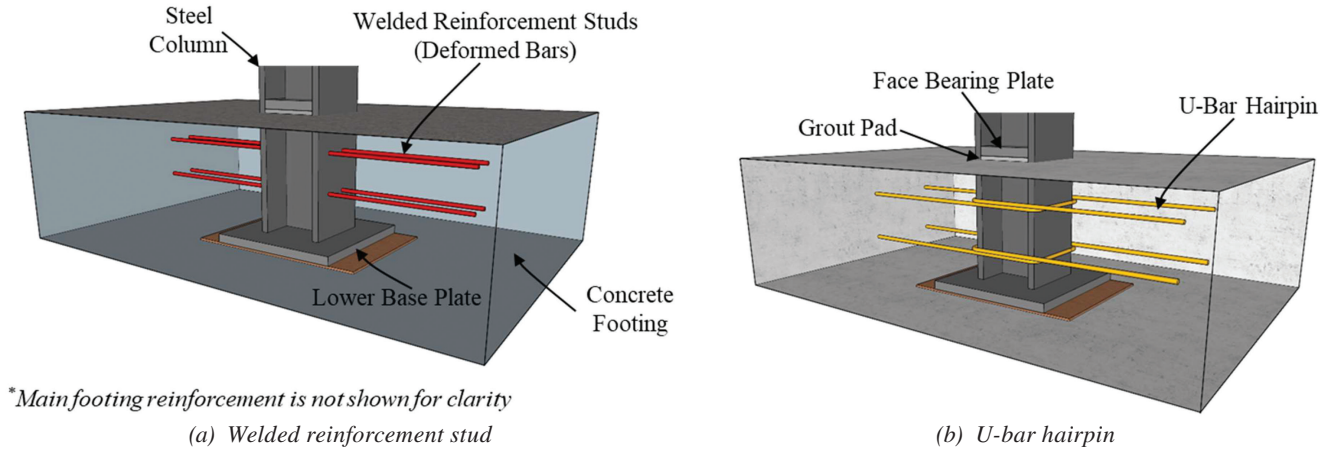

*Main footing reinforcement is not shown for clarity

(a) Welded reinforcement stud

(b) U-bar hairpin

Fig. 3. Details under investigation for the experimental program.

Mattock and Gaafar (1982). From the perspective of ECB connections, the following aspects of this method are problematic: (1) It assumes that the entire moment is carried solely by the bearing against the flanges (i.e., it does not consider the effect of the embedded base plate and its contribution to moment resistance); (2) the term reflecting the effect of concrete confinement is unbounded, which has the potential of overestimating the bearing stresses in concrete foundations, because footings are often significantly wider than the embedded steel section as compared to shear walls; and (3) several factors relating to the mechanics of the method (e.g., the ratio of the neutral axis location to the depth of embedment, c/L_e, and consequently the value k_2) have been particularized for simplification based on geometrical aspects and constraints that are not necessarily analogous for the case of ECB connections [see Figure 4(a)].

Grilli and Kanvinde (2017) developed a strength model that presumes that the total applied base moment is resisted by two mechanisms [see Figure 4(b)]: (1) horizontal bearing stresses against the column flange—assumed to be rectangular/constant in nature, accompanied by the formation of a shear panel action, and (2) vertical bearing stresses against the base plate that resist its rotation. The distribution of moments between these two mechanisms is determined through a semi-empirical equation that is inspired by the analytical solution to a beams-on-elastic foundations problems (Hetenyi, 1946), wherein the column is assumed to be a beam embedded in the elastic foundation. The details of these derivations are provided in Grilli and Kanvinde (2017); however, the equations are not as succinct as for the SDM approach.

Neither model accounts for the reinforcement attached to the column flanges (commonly used in practice), neither by ignoring its contribution (the AISC SDM model where the reinforcement is only prescribed for force transfer) nor by not accounting for its presence in the mechanical model through the equilibrium equations (as per Grilli and Kanvinde, 2017). This is problematic because the presence of additional reinforcement greatly influences the failure modes and the strength and stiffness of the connection. The next section presents an experimental program featuring ECB connections with reinforcement attachments. The results from the tested specimens are then compared with the available strength models presented previously to support the development of an approach that overcomes the limitations of these existing models.

EXPERIMENTAL PROGRAM

Figure 5 illustrates the test setup, and Figure 6 illustrates the specimen detailing. Table 1 summarizes the test matrix along with key experimental results.

Test Setup

Figure 5 shows the test setup, including the specimen. Specific aspects of the test setup and specimens are outlined in the following:

1. All specimens featured wide-flange cantilever columns. The height of load application (9.5 ft above the surface of concrete) was assumed to be the inflection point in a first-story column. The columns were all ASTM A992/A992M Grade 50 and were designed to remain elastic throughout the test.
2. Axial compression was introduced through a cross-beam assembly with two hydraulic jacks (shown in Figure 5) connected to tension rods and a freely rotating clevis. The axial forces did not introduce *P*-Δ moments.
3. The columns were placed on a plywood sheet with 1 in. thickness and the same plan dimensions of the lower base plate to reflect a supporting condition similar to a

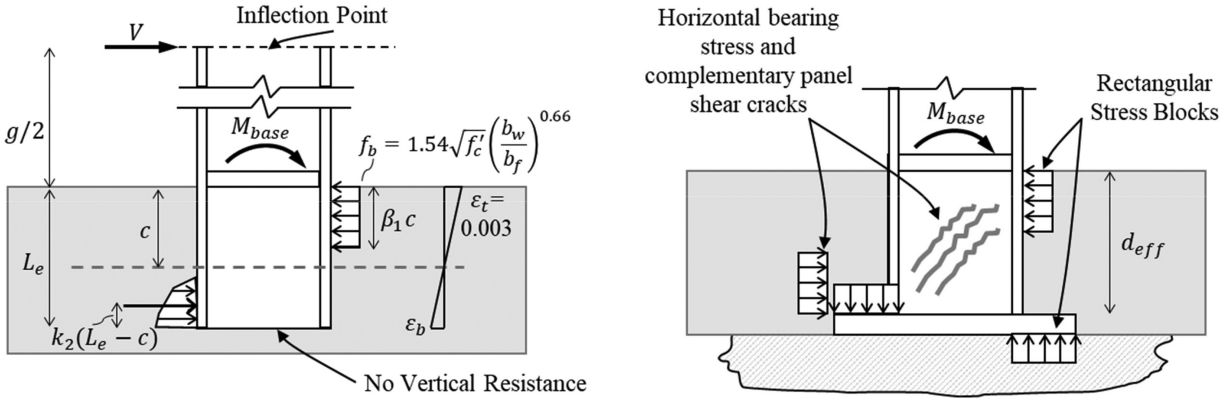

(a) AISC Seismic Design Manual *approach* *(b) Grilli and Kanvinde (2017) model*

Fig. 4. Strength model assumptions.

thin unreinforced slab for erection purposes, rather than directly bearing on bare soil.

4. Face-bearing plates similar to stiffeners were provided at the top of the embedment region (see Figure 6), consistent with the design practice. These provide a load path for compressive forces rather than transferring it through the bottom base plate, which often rests in an unreinforced slab.
5. The pedestals were fastened to the laboratory floor with pretensioned threaded anchors at a distance of 4.5 ft from the column to minimize boundary effects on the stress distribution and failure modes in the vicinity of the column.

Test Matrix

Referring to Table 1, the following test parameters were varied: (1) the configuration of the attached reinforcement—deformed bar anchor versus U-hairpin, (2) the cross-sectional area of the horizontal reinforcement, (3) the column size, and (4) the addition of supplemental vertical reinforcement (stirrups) through the length of the concrete pedestal. Parametric values of the test matrix were selected to reflect similarity with construction practice within the limitations of the test setup; specifically:

1. The column sections were selected to ensure failure in the connection rather than in the column. Thus, the columns are larger relative to the embedment depths in comparison to actual design cases in which the base would typically be stronger than the column.
2. Compressive axial loads were selected to be 10–20% of the axial yield capacity of a hypothetical column that would have an embedment depth similar to the ones used in the study; for more in-depth discussion of this, see Grilli et al. (2017).
3. The footing was similar to the specimens tested by Grilli et al. (2017) in terms of concrete dimensions and nominal reinforcement. All footings were provided with minimal longitudinal and transverse reinforcement. The column embedment depth, d_{embed}, footing dimensions, and footing reinforcement are illustrated in Figure 6.

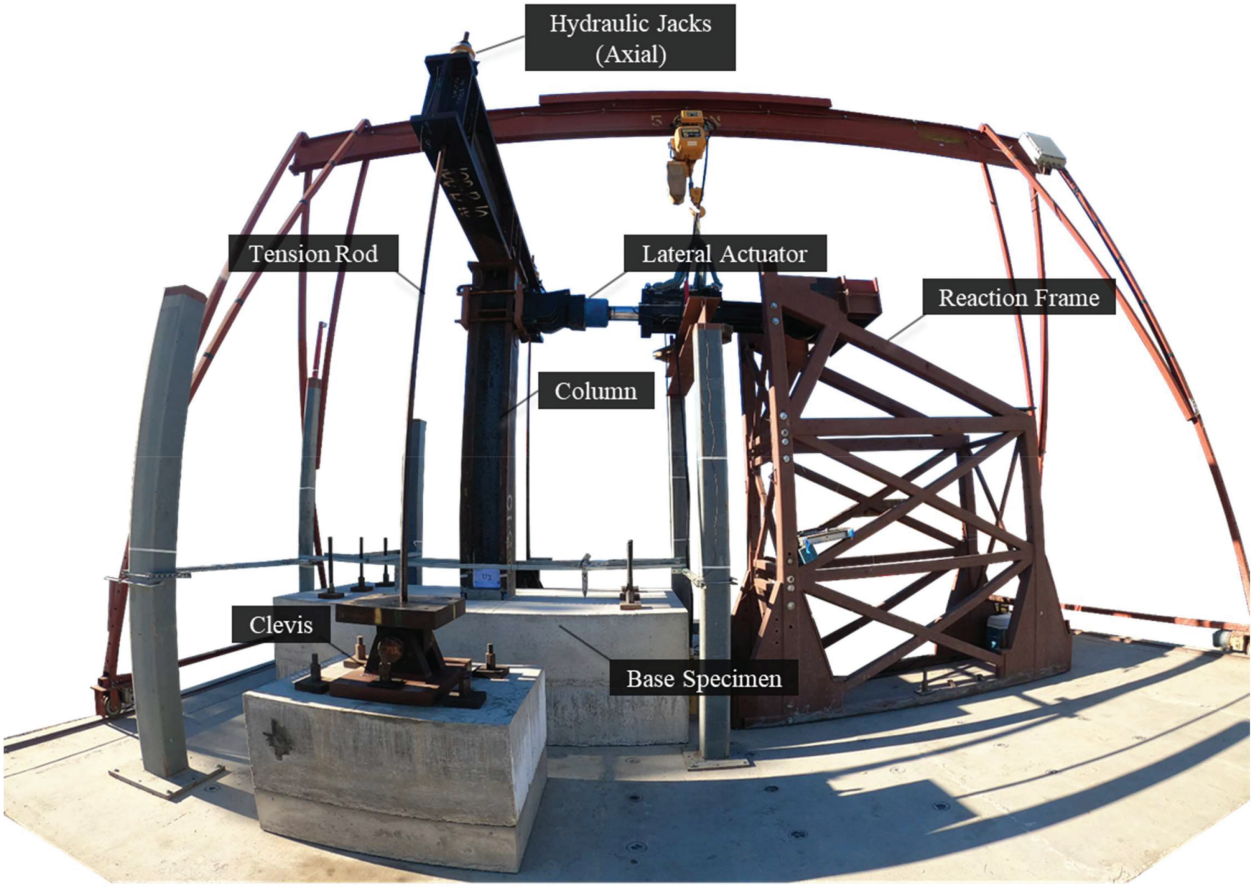

Fig. 5. Wide-angle view of test setup.

This is illustrated for the U-bar hairpin details; however, similar detailing and dimensions are used for the welded reinforcement detail (Test #1) previously shown in Figure 3(a).

4. Referring to Figure 6 and Table 1, reinforcement attachments details were installed in all specimens. All tests featured two rows of attached reinforcement bars (close to the face of the concrete footing). The attached reinforcement was fully developed in tension by providing an adequate tension development length as per ACI 318-19 (ACI, 2019). The location of the attached reinforcement was selected in accordance with the AISC *Seismic Provisions* and AISC *Seismic Design Manual* (AISC, 2016, 2018) such that (a) the first region (top row) of the attached reinforcement coincided with the

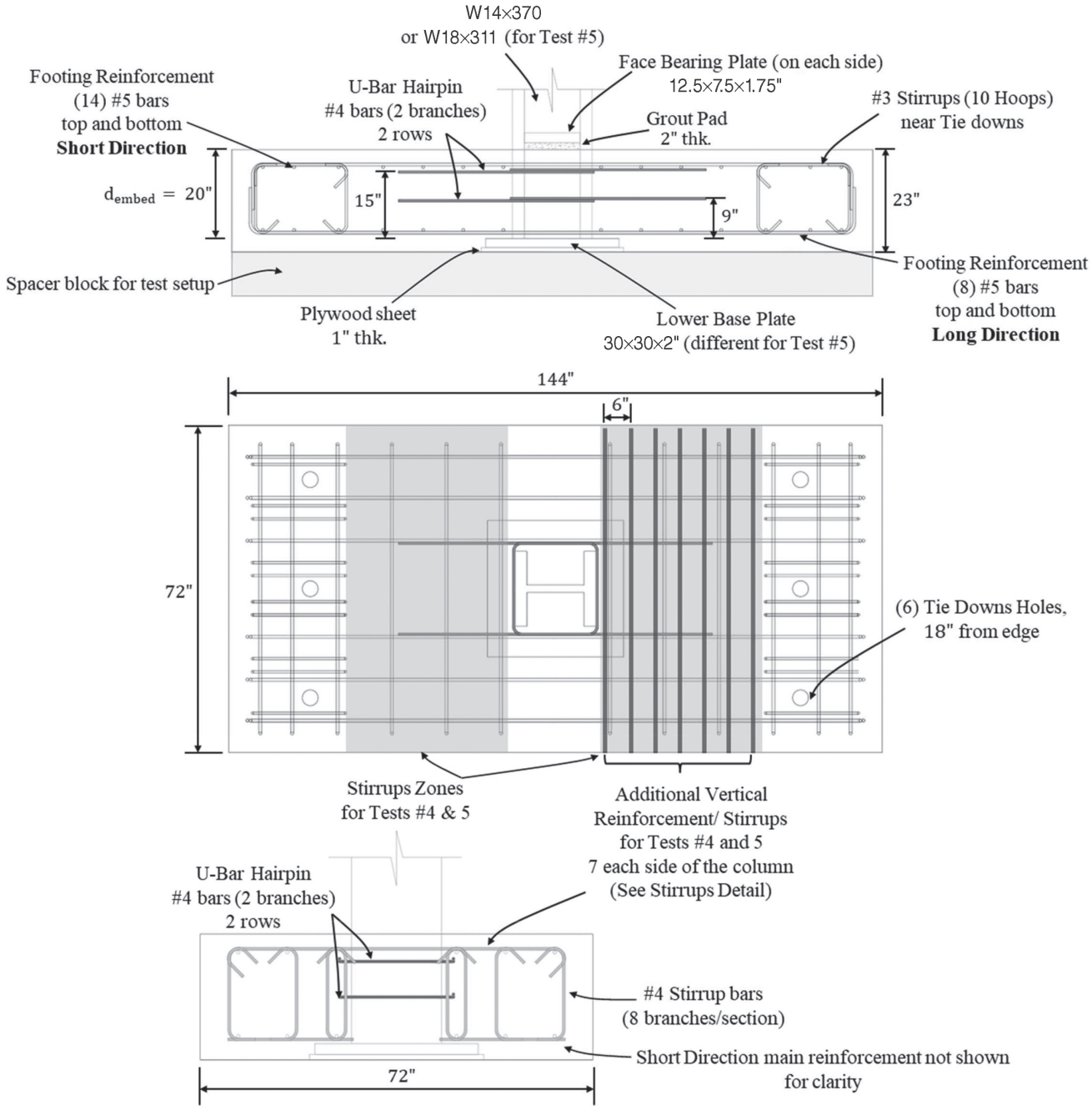

Fig. 6. Specimen detailing (see Table 1 for different parameters across the tests).

longitudinal footing reinforcing bars closest to the face of the foundation, and (b) the second region (bottom row) is placed at a distance no less than $d_{col}/2$ from the termination of the embedded length.

5. Test 1 included #4 (½-in.-diameter) weldable rebars (ASTM A706 Grade 60), arc welded directly to the flange [see Figure 3(a)], whereas Test 2 featured #4 (½-in.-diameter) U-bar hairpin reinforcement (ASTM A615 Grade 60) wrapped around the column embedment (alternating in each row to engage the flanges in both loading directions). Test 3 featured bundled U-bar hairpins with a total of 4 #6 U-bar hairpins per row (¾ in. diameter). For Tests 4 and 5, supplemental vertical reinforcement/stirrups (shown in Figure 6) were installed to assess the effect on connection strength and failure modes.
6. Subsets of tests may be considered to isolate the effect of test variables. For example, Tests 1 and 2 provide a direct examination of the effect of different attachment techniques (i.e., arc welding versus anchoring/fixing), whereas Tests 2 and 3 provide an investigation of the effect of reinforcement area/size. In addition, Tests 2 and 4 allow the investigation of the effect of vertical stirrups, whereas Tests 4 and 5 directly examine the effect of column width/size. The specimens from this program also allow for direct comparison with tests from the experimental program by Grilli et al. (2017), which featured otherwise similar column sizes and footing dimensions.

Standard cylinder tests were performed for all concrete pours as well as grout for all specimens. Coupon tests from the attached reinforcement (both welded studs and U-bar hairpins) used in the experiments were also conducted. Table 2 summarizes the results of ancillary tests for measured material properties that are used to interpret results.

Loading Protocol

For all test specimens, the axial compression was introduced and held constant while the lateral deformation history (expressed in terms of column drift ratio) was applied as per the ATC-SAC protocol (Krawinkler et al., 2000). This protocol was applied until 6% drift amplitude was reached except for Tests 1 and 2, which were stopped at 5% drift.

EXPERIMENTAL RESULTS

Figures 7(a)–7(e) show the moment-drift response of all the five specimens. Figures 8(a)–8(c) show photographs of damage progression and failure modes for the tested specimens, whereas Table 1 shows key results. A qualitative assessment of experimental response for the tested specimens is now presented, to facilitate the interpretation of quantitative data, which is presented subsequently. In the following discussion, the terms "ahead of the column" and "behind the column" denote the compression side of the connection (i.e., in the direction of applied load) and the tension side of the connection, respectively.

Qualitative Discussion of Failure Modes

Referring to Figures 8(a)–8(c), all specimens followed a qualitatively similar damage progression, with some variations resulting from reinforcement detailing. During the initial stages of loading (applied drift less than 1%), minor cracks initiated at the corners of the column as shown in Figure 8(a). Following this, diagonal shear cracks formed on the sides of the block, accompanied by a vertical crack in the concrete behind the column flange, where the attached reinforcement produces tension. These cracks grew in width as loading progressed, with spalling of the concrete ahead of the column flanges. These vertical cracks behind the column reduce the uplift capacity of the base plate, as discussed later. As the applied drift increased, the diagonal shear cracks on the sides of the concrete block grew in width indicating the development of a shear panel. However, this did not control failure or the peak load. The final failure mode, which controlled connection strength, varied from one specimen to another, depending on the vertical reinforcement (or its absence). One of two scenarios occurred [shown photographically in Figures 8(b)–8(c)], these are:

1. In Tests 1, 2, and 3 (without the additional vertical reinforcement), final failure was accompanied by vertical breakout on the tension side of the connection. This failure mechanism is similar to anchor pryout failure modes in concrete (Anderson and Meinheit, 2005), which was observed in similar details by Grilli et al. (2017); see Figure 2(b). The pryout failure occurs when the moment resisting the uplift of the base plate reaches a critical value. This results in the formation of a breakout cone, as shown in Figure 8(b).
2. For Tests 4 and 5 (with additional vertical reinforcement as shown in Figure 6), the presence of supplemental reinforcement mitigated the final tension breakout failure. Instead, the failure occurred at the interface of the vertical crack forming behind the column flanges, as shown in Figure 8(c), at a location between installed stirrups. No spreading of failure (i.e., cone formation) was observed for such tests.

In all tests, the peak moment was achieved between 2% to 2.5% drift. After this, strength deterioration was observed [see Figures 7(a)–(e)] as the breakout block of concrete started to separate from the remainder of the footing. A qualitatively similar response—in other words, pinched hysteresis with excellent deformation capacity and minimal

Table 1. Tests Matrix and Key Results

Test[a]	Axial Load P (kips)	Column Size b_f (in.)	Embedment Depth d_{embed} (in.)	Z[b] (in.)	Base Plate $t_p \times N \times B$ (in.)	Attached Reinforcement Grade	Reinforcement Configuration	M_{max+}^{test} (kip-ft)	M_{max-}^{test} (kip-ft)	$\frac{M_{max}^{test}}{M_{max}^{AISC\ SDM}}$[c]	$\frac{M_{max}^{test}}{M_{max}^{Model}}$
1	100	W14×370 (16.5)	20	114	2×30×30	Weldable rebar studs ASTM A706 Grade 60	(4) #4 (½ in. diameter)	994	1002	0.77	0.82
2	100			114		U-bar hairpin ASTM A615 Grade 60		1055	904	0.81	0.88
3	100			114			(8) #6 (¾ in. diameter)	1334	1109	1.03	1.06
									Mean	**0.87**	**0.92**
									CoV	**0.16**	**0.14**
4	100			114	2×30×30	U-bar hairpin ASTM A615 Grade 60	(4) #4 (½ in. diameter) + Vertical reinforcement	1196	908	0.92	0.90
5	100	W18×311 (12)			2×34×28			1220	820	1.05	1.01
									Mean	**0.99**	**0.96**
									CoV	**0.09**	**0.08**
1G	100	W14×370 (16.5)		112	2×30×30	–	–	1902	1927	1.45	1.22
2G	100	W18×311 (12)		112	2×34×28			1714	1599	1.44	1.17
3G	–	W14×370 (16.5)	30	122	2×30×30			2759	2540	0.97	0.91
4G	100			122				3042	2664	1.07	0.99
5G	150 (T)			122				2803	2555	0.99	0.95
									Mean	**1.19**	**1.05**
									CoV	**0.20**	**0.13**
									Mean (All)	**1.05**	**0.99**
									CoV (All)	**0.22**	**0.13**

[a] New tests are labeled from 1–5, whereas tests from Grilli et al. (2017) are labeled 1G–5G.
[b] Moment-to-shear ratio (i.e., distance from point of load application to top of concrete); see Figure 9(c).
[c] M_{max}^{test} is the maximum moment value of both directions of loading (positive and negative).

Table 2. Summary of Measured Material Strengths from Ancillary Tests					
Test	Number of Samples[a]	Yield Strength F_y^{rebar} [b] (ksi)	Ultimate Strength F_u^{rebar} (ksi)	Concrete Compressive Strength f_c' [c] (ksi)	Grout Compressive Strength F_{grout} [c] (ksi)
ASTM A706 Grade 60 reinforcement	2	71.2	94.2	–	–
ASTM A615 Grade 60 reinforcement	2	65.0	102.5	–	–
Concrete cylinders	5	–	–	4.0	–
Grout cylinders	4	–	–	–	8.5

[a] Average values for tested samples are presented.
[b] Measured yield stress for ASTM A706 bars is based on the 0.2% offset method.
[c] Compressive strength for concrete and grout cylinders is measured on the day of full-scale test.

strength degradation (i.e., less than a 20% drop in peak base moments at 4% drift)—was observed for all tests, except for Test 3 (with bundled U-bar hairpins), which showed a drop in load of roughly 40% after achieving capacity at around 3% drift.

Quantitative Analysis of Test Data

Table 1 summarizes key quantities measured in the experiments. Two moment values were recovered for each test corresponding to maximum moment observed in each loading direction. These are denoted as M_{max+}^{test} and M_{max-}^{test}, such that the positive sign denotes the direction of the first

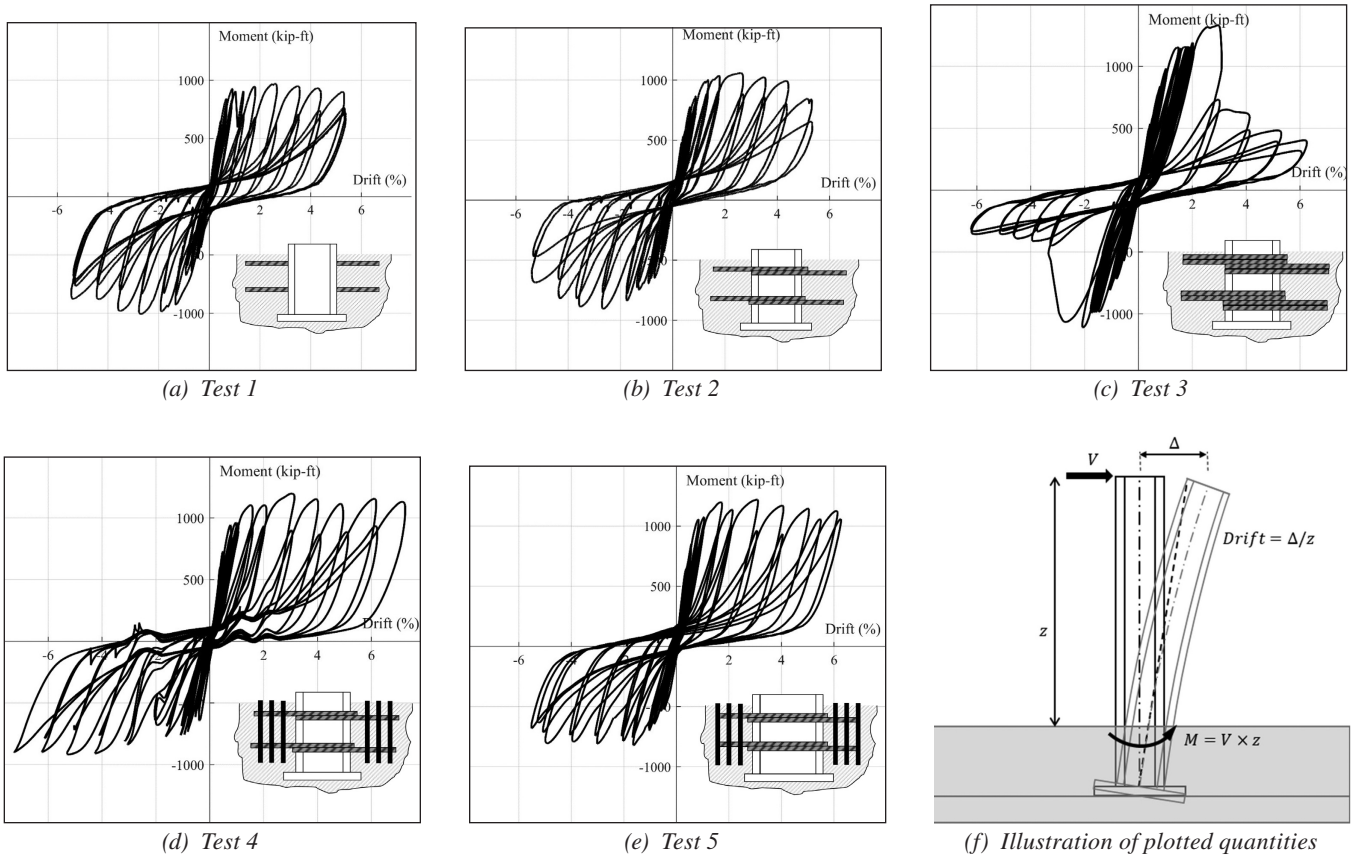

(a) Test 1 (b) Test 2 (c) Test 3

(d) Test 4 (e) Test 5 (f) Illustration of plotted quantities

Fig. 7. Moment-drift plots for all tests and a schematic illustration of plotted quantities.

deformation excursion. Referring to Table 1 and Figures 7 and 8, the following observations may be made:

1. The main observation is that the application of horizontal reinforcement (i.e., attached reinforcement to column flanges) significantly reduced the strength and stiffness relative to values observed by Grilli et al. (2017). Specifically, the specimens from Tests 1 and 2 of the Grilli et al. (2017) test program (Test 1G and 2G in Table 1) are nominally identical to Tests 1 and 5 of this study except for the attachment of horizontal reinforcement. On average, the strengths observed in the specimens with horizontal reinforcement is 45–50% lower than that of their unreinforced counterparts [see Figure 8(d)]. This is counterintuitive and a somewhat disquieting observation. However, a closer evaluation of the underlying mechanisms and failure mode suggests that this may be attributed to the development of a tension field in the concrete behind the column due to the horizontal reinforcement that is in tension. This tension field reduces the resistance of the concrete to uplift of the base plate, significantly reducing overall connection strength.
2. A comparison of results from Tests 1 and 2 (welded rebar stud versus U-bar hairpin) indicates that the moment strength observed in both tests is very close (within 5%), while the load-deformation shows modest difference in terms of cycle-to-cycle degradation.
3. A comparison between Tests 2 and 4 provides a direct assessment of the effect of additional vertical reinforcement/stirrups. The stirrups increase the strength of the connection by 20%. This may be attributed to the fact that the vertical reinforcement mitigates the formation of the tension breakout cone, resulting in higher moment resistance.
4. Comparing Tests 4 and 5 (which are similar in terms of embedment depth, attached reinforcement, and stirrups, but differ in terms of column section and base plate geometry; see Table 1), the strengths are almost identical.

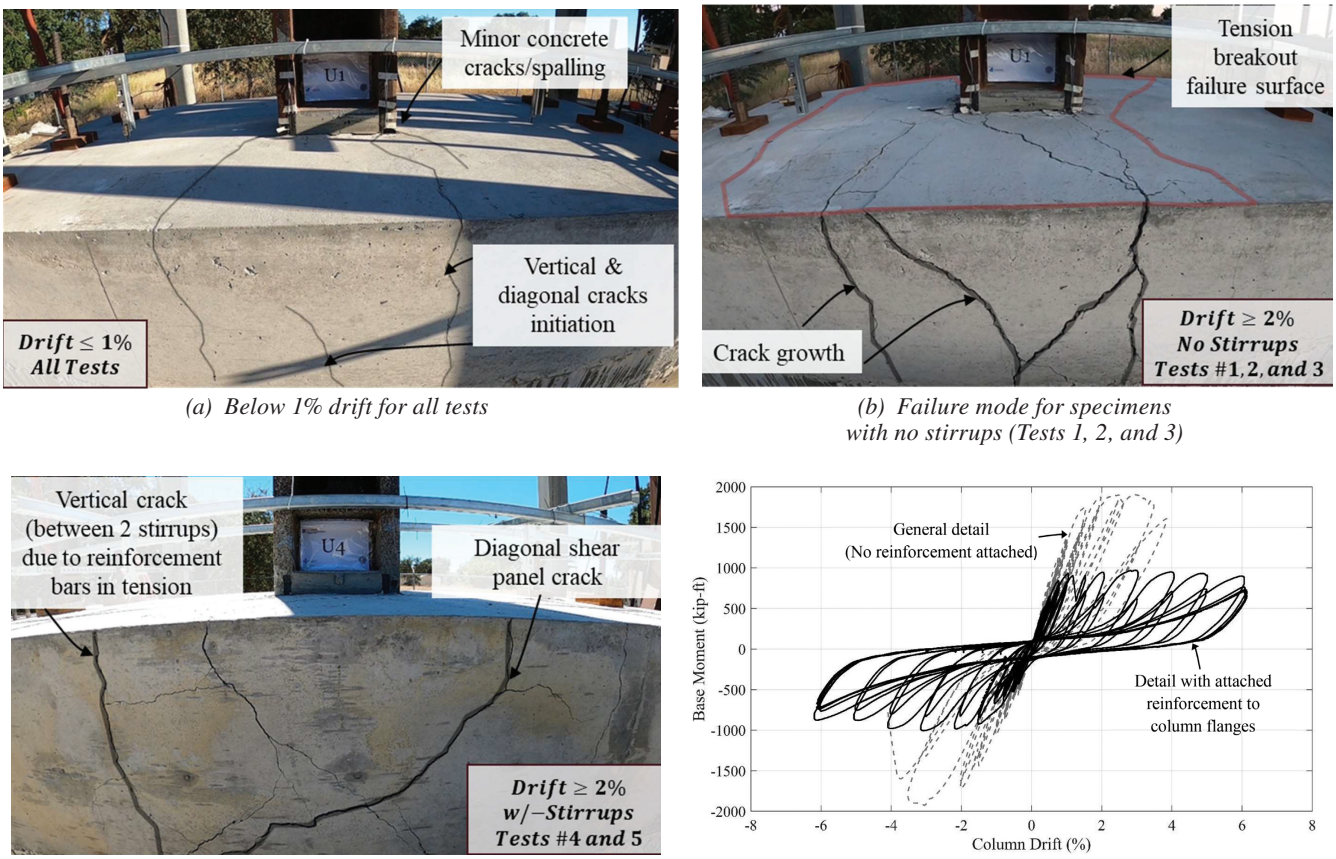

(a) Below 1% drift for all tests

(b) Failure mode for specimens with no stirrups (Tests 1, 2, and 3)

(c) Failure mode for specimens with stirrups (Tests 4 and 5)

(d) Moment-drift curve showing the effect of additional horizontal reinforcement

Fig. 8. Typical damage progression and behavioral insights.

5. The effect of additional attached horizontal reinforcement may be assessed through Tests 2 and 3, which differ only in terms of the cross-sectional area provided by the attached horizontal reinforcement. A 20% increase in moment capacity was observed in Test 3, which has a 340% higher cross-sectional area of reinforcement.

6. All specimens with reinforcement attained very high deformation without significant loss in moment strength (i.e., 6% drift compared to about 3% for the specimens without reinforcement tested by Grilli et al., 2017).

PROPOSED MODEL FOR STRENGTH CHARACTERIZATION

Based on the observations from the experimental program, this section describes the development of a strength model for ECB connections. The model incorporates observations from all relevant test data on embedded connections to quantify internal force transfer mechanisms and failure modes. Specifically, the model considers specimens from this study (with additional horizontal reinforcement), as well as those tested previously by Grilli et al. (2017) without such reinforcement, and provides a unified approach to characterize their strength. The proposed approach assumes that the various internal mechanisms act "in parallel," similar to the development of a plastic mechanism within the connection. This is based on the observation (across all experiments) that significant deformations are mobilized within the various mechanisms (horizontal and vertical bearing, as well as shear panel) such that the strengths from these may be considered additive. Furthermore, this results in a simplified model that also provides fairly accurate results. Figures 9(a)–9(d) schematically illustrate the internal stress distributions and force transfer mechanisms, whereas Figures 9(e)–9(f) illustrate failure modes corresponding to the vertical breakout/pryout limit states. Figure 10 includes a flowchart summarizing the process to determine the ECB connection capacity using the proposed model.

Moment Resistance Due to Horizontal Bearing Stresses

Referring to Figure 9(c), one fraction of the applied moment, M_{HB}, and the entire shear, V, is resisted through the development of bearing stresses on both sides of the embedded column flanges. A modified version of the previously discussed approach developed by Grilli and Kanvinde (2017) is used to estimate the moment resistance provided by the horizontal bearing mechanism while adding the contribution of horizontal reinforcement. The bearing stresses are idealized such that a uniform stress distribution is assumed for both the top stress, f_b^{top}, and the bottom stress, f_b^{bottom}, such that:

$$f_b = f_b^{top} = f_b^{bottom} = 1.54\sqrt{f_c'}\left(\frac{b_w}{b_f}\right)^n \le 1.7f_c' \tag{2}$$

The term b_w/b_f accounts for the effect of confinement, wherein b_w is the width of the foundation, and b_f (in inches) is the width of the flange. The exponent, n, is calibrated based on experimental data to a value of $n = 0.66$ (Mattock and Gaafar, 1982). The value of bearing stress is capped by a value of $1.7f_c'$, reflecting the maximum confinement of the concrete by the reinforcement and the surrounding concrete. Referring to Figure 9(c), the resultant compressive forces C_{top} and C_{bottom} are defined as follows:

$$C_{top} = f_b^{top}\beta_1 c b_j \tag{3}$$

$$C_{bottom} = f_b^{bottom}\beta_1 (d_{embed} - c) b_j \tag{4}$$

In Equations 3 and 4, c (in inches) is the neutral axis depth, $\beta_1 = 0.85$ is the factor relating the depth of the equivalent rectangular stress block to c, and $b_j = (b_f + B)/2$ is the effective width of the joint panel, where B is the width of the lower base plate. Based on work by Grilli and Kanvinde (2017), this expression reflects the development of bearing stresses over a width greater than the column flange because a portion of the concrete panel outside the flange is mobilized. The attached reinforcement is assumed to act in tension and compression in the case of the welded reinforcement bars, and only in tension in the case of the U-bar Hairpin, since the column can transfer force to it only by bearing against the wraparound segment of the U-bar. The reinforcement bars are assumed to be elastic-perfectly-plastic and fully developed in tension (as per ACI 318-19), $F_{rebar} = A_{rebar} \times F_y$. The resultant from each rebar row is directly added to the resultants from the stress distributions, and the moment resistance due to horizontal stresses, M_{HB}, may be obtained by summation of the resultant moments at the top of foundation level, such that:

$$V - C_{top} + C_{bottom} - F_{rebar}^{top} + F_{rebar}^{bottom} = 0 \tag{5}$$

$$M_{HB} = -C_{top}\frac{\beta_1 c}{2} + C_{bottom}\left[d_{embed} - \frac{\beta_1 (d_{embed} - c)}{2}\right] - F_{rebar}^{top} d_{rebar}^{top} + F_{rebar}^{bottom} d_{rebar}^{bottom} \tag{6}$$

In Equations 5 and 6, F_{rebar}^{top} and F_{rebar}^{bottom} are the resultant forces from the engaged reinforcement rods, and d_{rebar}^{top} and d_{rebar}^{bottom} are the distances from the rebar location to the top of the foundation surface for the top and bottom rebar, respectively. Eliminating the term c, which is common to both Equations 5 and Equation 6 (through the resultant force terms C_{top} and C_{bottom}), results in one expression relating the moment capacity due to horizontal bearing directly to the shear force:

$$M_{HB} = \frac{(F_{rebar}^{top} - F_{rebar}^{bottom} - V)d_{embed}}{2} - \frac{(F_{rebar}^{bottom} - F_{rebar}^{top} + V)^2}{4b_j f_b} - \frac{\beta_1 b_j d_{embed}^2 f_b(\beta_1 - 2)}{4} - F_{rebar}^{top} d_{rebar}^{top} + F_{rebar}^{bottom} d_{rebar}^{bottom} \quad (7)$$

Equation 7 represents an interaction equation between the shear force, V, and the moment, M_{HB}, such that for any given shear force V, the maximum moment may be determined using it. The equation assumes that the "neutral axis"—the transition in bearing stress direction—occurs between the upper and lower layers of horizontal reinforcement. Further, it is noted that the moment determined in this manner is calculated at the elevation corresponding to the top of the footing.

Moment Resistance Due to Vertical Bearing Stresses

Referring to Figure 9(d), the base plate at the bottom of the embedment is subjected to bearing stresses on the lower and upper surfaces, resisting the moment transferred to the base through the column flanges, as well as the net axial force transferred to the base plate. The base plate is assumed to resist the total axial force (through upward bearing in the case of compressive load or downward bearing in the case of tensile load) in addition to the moment resisted through the vertical bearing mechanism, M_{VB}. Observations from experiments suggest that although the face-bearing plate at the top of the foundation transfers axial compression into the footing, the separation between the column and the footing during lateral loading [see Figures 8(b)–8(c)] implies that a significant portion of this axial load is carried through the

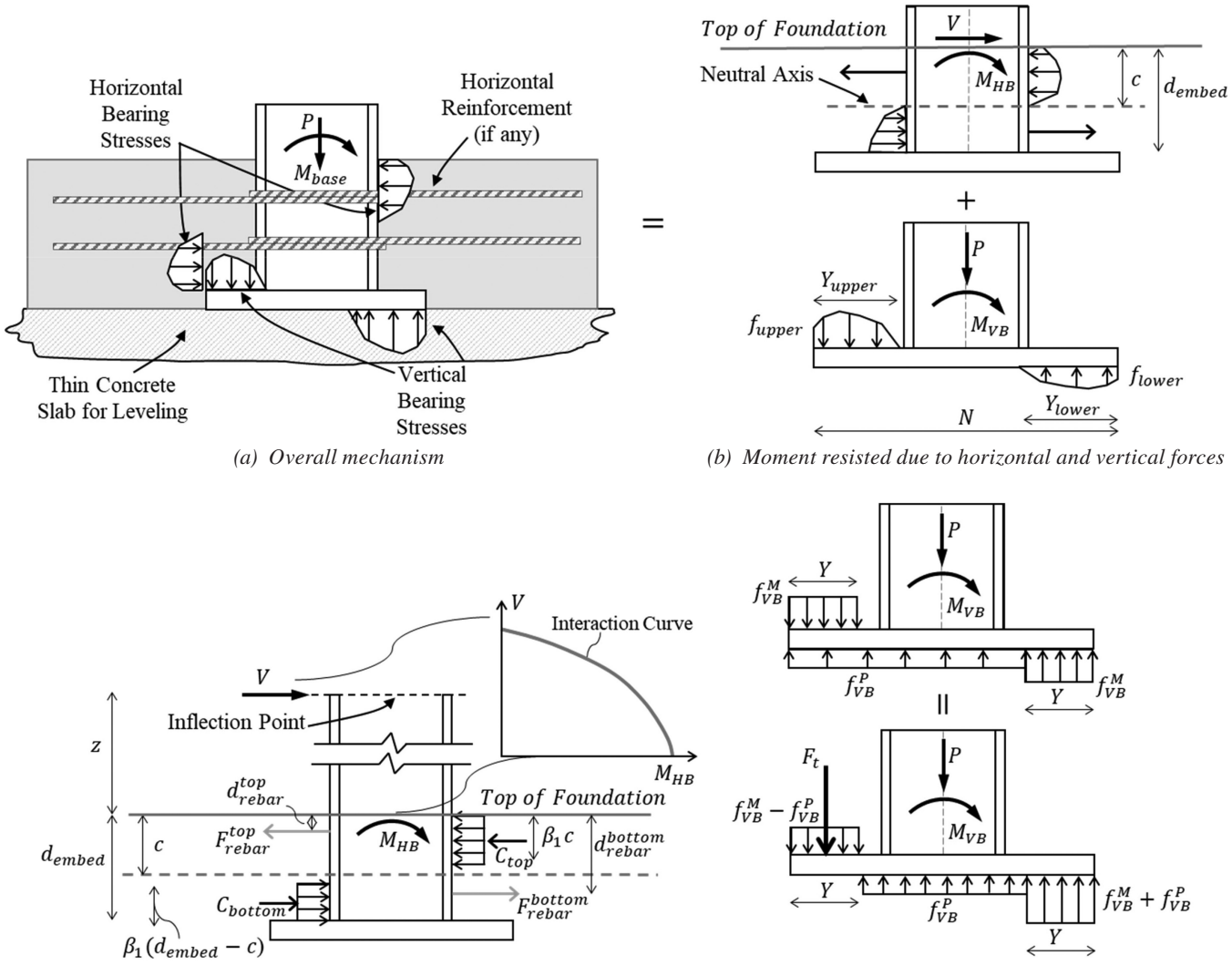

(a) Overall mechanism

(b) Moment resisted due to horizontal and vertical forces

(c) Horizontal resistance mechanism

(d) Idealized vertical resistance mechanism

Fig. 9(a–d). Proposed model for strength characterization.

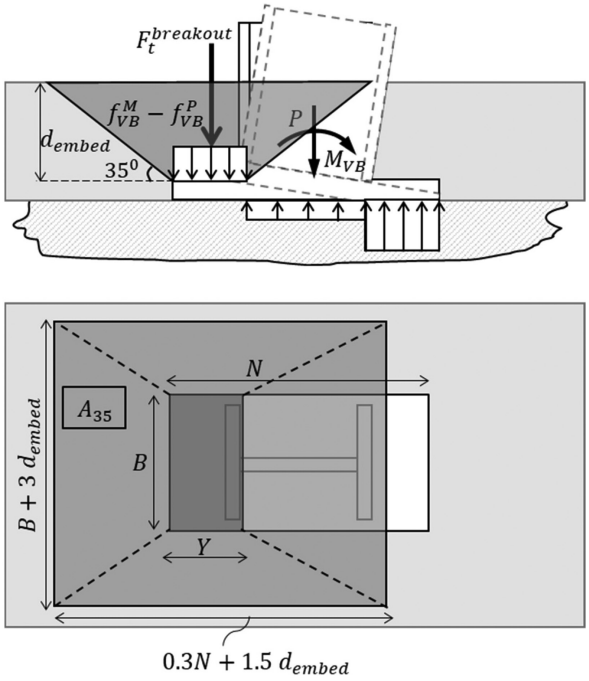

(e) Tension breakout failure mode (vertical bearing)

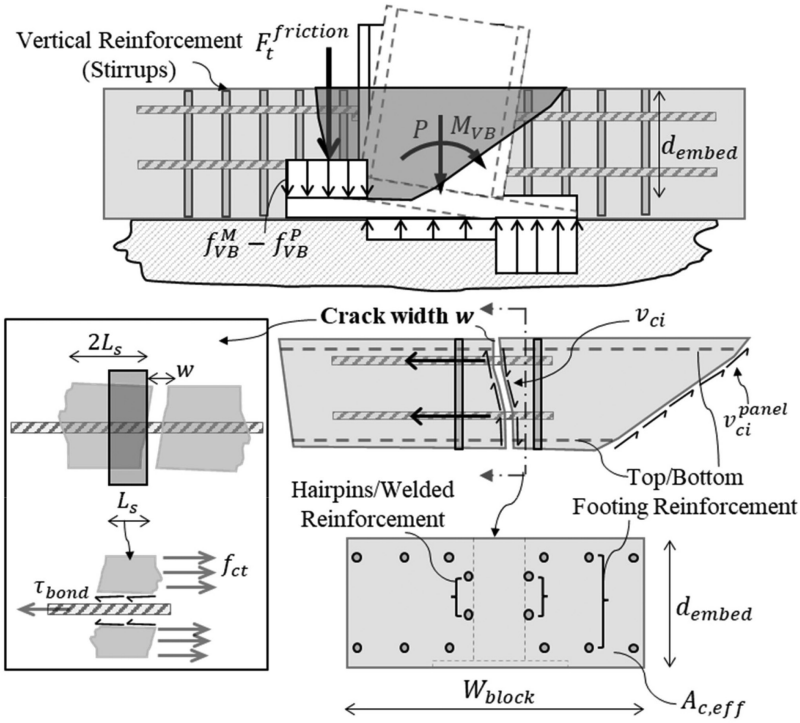

(f) Shear/friction failure mode (vertical bearing)

Fig. 9(e–f). Proposed model for strength characterization.

footing to the base plate at the bottom. The stress distribution on the base plate itself arises from a superposition of stresses due to axial forces and the moment, M_{VB} (Grilli and Kanvinde, 2017), and idealized these stresses as a stepped distribution [see Figure 9(d)], to reflect the combination of axial force and bending resisted by them. The width, Y, of the two "outside" steps was $0.3N$, whereas the middle step was $0.4N$ wide. This results in a stress distribution with values determined using Equations 8 and 9. Specifically, the stresses on the tension side, $f_{VB}^{M} - f_{VB}^{P}$, on the compression side step, $f_{VB}^{M} + f_{VB}^{P}$, and on the central portion may be related to the applied loading as follows:

$$f_{VB}^{M} = \frac{M_{VB}}{(N-Y)\times Y \times B} \tag{8}$$

$$f_{VB}^{P} = P/(B\times N) \tag{9}$$

Under these stresses, critical failure mode in the lab specimens was observed to be the breakout/pryout of the concrete on the tension side of the connection. This assumes that the supporting material slab below the base plate can develop the bearing stresses, $f_{VB}^{M} + f_{VB}^{P}$, induced on the compression side without failure. Implications of disregarding vertical bearing failure on the compression side of the connection are discussed later. With this assumption, determination of the moment, M_{VB}, requires estimation of the force, F_t, that results in a breakout/pryout type failure of the concrete above the base plate on the tension side:

$$F_t = \left(f_{VB}^{M} - f_{VB}^{P}\right)(Y\times B) \tag{10}$$

Following the idealization of Grilli and Kanvinde (2017), this force is assumed to act at a location of $Y/2$ (i.e., $0.3N/2$) from the edge [i.e., at the center of the outside step as shown in Figure 9(d)]. Utilizing the stress distributions in Equations 8–10, the following relationship may be obtained between the moment M_{VB} and the force F_t.

$$M_{VB} = \left(F_t - \frac{PY}{N}\right)(N-Y) \tag{11}$$

The magnitude of F_t may be estimated based on the failure mode, which in turn depends on the connection detailing. Based on the experimental results, three possible scenarios are now discussed.

Scenario 1: Breakout of concrete failure cone in the absence of attached horizontal reinforcement

This failure mode is applicable only when no horizontal reinforcement is attached (tests by Grilli et al., 2017); that is, the tension field produced by the reinforcement does not affect the development of such a cone. In such a case, as shown in Figure 9(e), the total breakout force may be calculated as:

$$F_t = F_t^{breakout} = \frac{40}{9}\frac{1}{\sqrt{d_{cover}}}\sqrt{f_c'}A_{35} \tag{12}$$

Equation 12 is based on the concrete capacity design (CCD) method proposed by Fuchs et al. (1995), such that d_{cover} is the thickness of the material that must be ruptured for breakout, which is equal to d_{embed} for tension breakout. The term A_{35} is the projected area of a 35° failure cone emanating from the edges of the stress block on the tension side of width $0.3N$. The projected area A_{35} is shown in Figure 9(e) and is calculated using Equation 13:

$$A_{35} = (B + 3\ d_{embed})(0.3\ N + 1.5\ d_{embed}) - (B\times 0.3N) \tag{13}$$

Once established this way, the moment resisted through vertical bearing may be determined by using Equations 11–13.

Scenario 2: Breakout of concrete failure cone in the presence of attached horizontal reinforcement

As previously discussed, once reinforcement is attached to the column flanges, a tension field is created above the uplifting end of the base plate, reducing the resistance to vertical motion. Experimental data (from Tests 1–3 of this study) suggests that this resistance is negligible, such that the moment due to vertical bearing resistance may be conservatively assumed as zero (i.e., $M_{VB} = 0$).

Scenario 3: Shear failure of concrete in the presence of horizontal reinforcement and vertical stirrups

The third scenario is associated with the presence of vertical reinforcement/stirrups supplementary to the attached horizontal reinforcement. The intent of the stirrups is to increase the vertical bearing resistance by mitigating the breakout failure mode noted in Scenario 2. Referring to the test results and Figures 7(d)–7(e), the stirrups added a fair amount of vertical resistance while shifting the failure mode from a cone breakout into a direct shear failure at the weak point in the foundation [i.e., the cracked section between two stirrups as shown in Figure 8(c)]. For this, F_t may be estimated from the free-body diagram of the breakout block shown in Figure 9(f). This requires the determination of the shear stress on the crack interface. Cracks occurring along the interface between the cement paste and the aggregate particles result in a rough surface that can transfer shear through aggregate interlocking, as shown in Figure 9(f). Vecchio and Collins (1986) developed a relationship between the shear stress transferred across the crack, v_{ci}, the crack width, w, and the compressive stress, f_{ci} (in psi), on the crack, such that:

$$v_{ci} = 0.18\ v_{ci,max} + 1.64\ f_{ci} - 0.82\ \frac{f_{ci}}{v_{ci,max}} \tag{14}$$

where $v_{ci,max}$ (in psi) is the maximum shear stress that can be transferred across a crack when its width is w (in inches), given by:

$$v_{ci,max} = \frac{2.16\sqrt{f_c'}}{0.3 + \left(\frac{24w}{a + 0.63}\right)} \quad (15)$$

In Equation 15, a (in inches) is the diameter of the coarse aggregate in the cracked concrete, taken as 0.75 in. Given that the crack, as shown in Figure 9(f), is subjected to tension, f_{ci} in Equation 14 is zero, and thus:

$$v_{ci} = 0.18\, v_{ci,max} \quad (16)$$

The diagonal crack is assumed to have zero shear strength [v_{ci}^{panel} in Figure 9(f) at the right-hand side of the breakout block] because it has already opened completely due to shear panel action by the time the connection capacity is attained. The crack width, w, is determined from the bond-slip relationship at the reinforced concrete interface using the CEB-FIP Model Code (FIB, 1990). Using this approach, the crack width is:

$$w = 2\, L_s\, (\varepsilon_{sm} - \varepsilon_{cm}) \quad (17)$$

where $2L_s$ is the maximum slip length and ε_{sm} and ε_{cm} are the average value of steel and concrete strains, respectively. The transfer length, L_s, is defined as:

$$L_s = \frac{f_{ct} A_{c,eff}}{\tau_{bond} \sum \pi d_i} \quad (18)$$

where f_{ct} is the tensile strength of concrete (taken as $7.5\sqrt{f_c'}$ following the ACI 318-19 provisions); $A_{c,eff}$ (in square inches) is the effective area of concrete $W_{block} \times d_{embed}$ [see

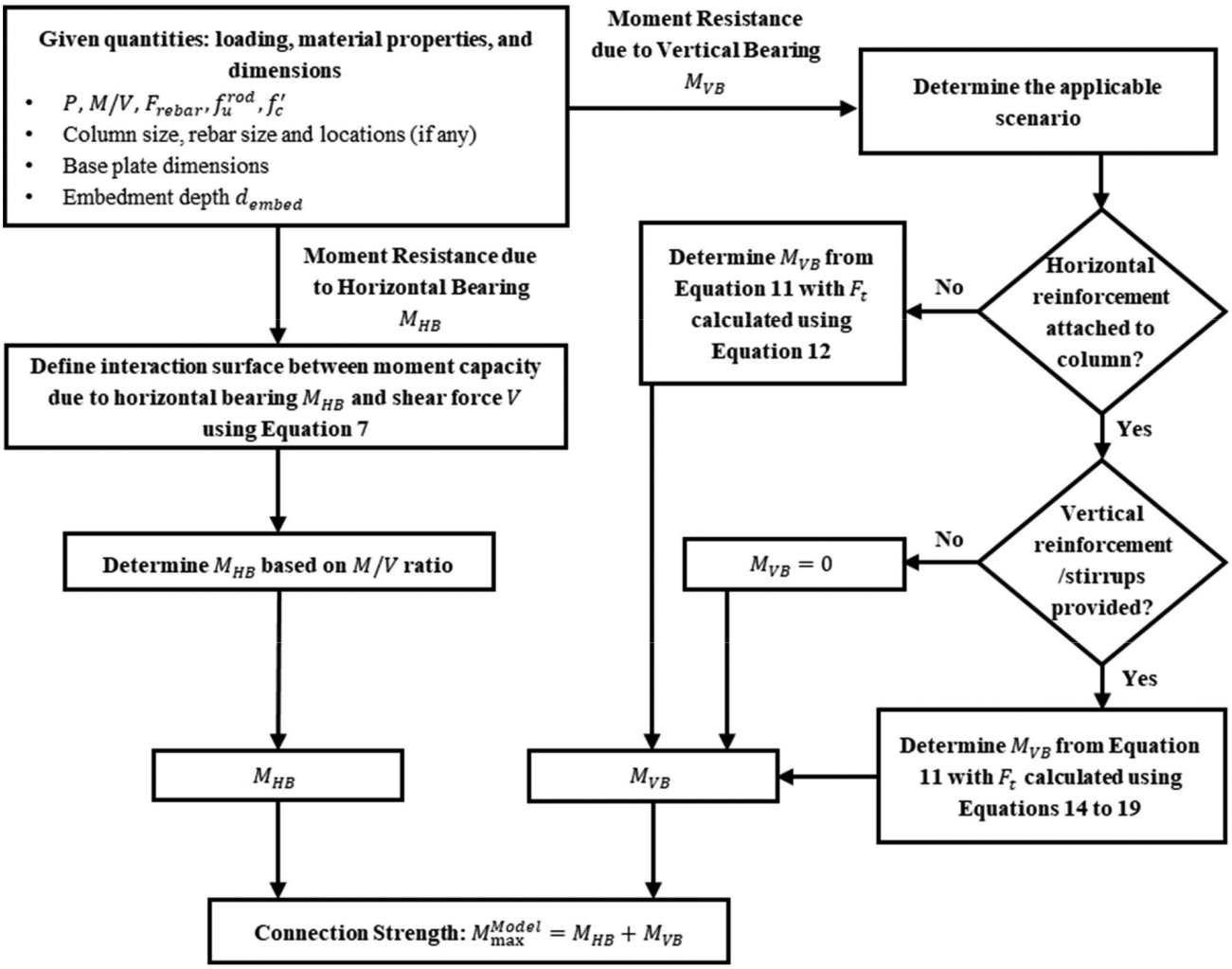

Fig. 10. Flowchart illustrating the strength characterization process.

Figure 9(f)] such that W_{block} is the width of the concrete foundation block; τ_{bond} (in ksi) is the average bond strength along the transfer length, taken as $0.95\sqrt{f_c'}$ (ksi) based on canonical literature (FIB, 1990); and d_i represents the diameters of bars crossing the considered crack. This includes the foundation main longitudinal reinforcement bars, shown in Figure 6, as well as the attached reinforcement, as shown in Figure 9(f). Once determined in this manner, the value of the upward force due to shear friction/aggregate interlocking across the cracked section may be calculated as:

$$F_t = F_t^{friction} = (v_{ci})(A_{c,eff}) \tag{19}$$

This value may then be substituted into Equation 11 to calculate the vertical moment capacity for the connection where vertical/stirrups reinforcement are provided. Once M_{VB} has been determined using the appropriate scenario, the connection strength may be estimated using the proposed unified model as:

$$M_{max}^{Model} = M_{HB} + M_{VB} \tag{20}$$

It is noted here that the moment determined in this manner reflects the moment at the elevation corresponding to the top level of the foundation, considering the statics used in determining M_{HB}. Because the determination of M_{VB} does not include any horizontal forces, it may be statically transferred from the bottom to the top of foundation.

RESULTS AND DISCUSSION

Table 1 summarizes the test-to-predicted ratios for the strength estimates $M_{max}^{test}/M_{max}^{Model}$ for all test data points using the methodology prescribed in the previous section. Also included in Table 1 are the test-to-predicted ratios for the connection strength calculated as per the AISC SDM model $M_{max}^{test}/M_{max}^{AISC\ SDM}$, which is the only model for which official design guidance exists. Figures 11(a) and 11(b) plot the test-to-predicted ratios from both models against the column embedment depth (normalized by the depth of the column, i.e., d_{embed}/d_{col}). Similar comparisons of test data to other models, including the variants of the Grilli and Kanvinde (2017) model are presented in Hassan et al. (2022). Referring to Table 1 and Figure 11, it is observed that:

- The average test-to-predicted ratio for the AISC SDM approach is 1.05 with a coefficient of variation (CoV) of 0.22, indicating that the method is conservative when considered across all the test data (although with large scatter). However, a closer inspection of the data indicates that the method is conservative for the generic details—that is, the Grilli and Kanvinde (2017) tests without horizontal reinforcement—because it does not incorporate the effect of vertical bearing (average test-predicted ratio = 1.19). However, where vertical bearing is insignificant (i.e., tests from the current study without stirrups), the results are somewhat less conservative (average test-predicted ratio = 0.87), while for the cases with the stirrups, the method is fairly accurate, even if it does not consider the contribution from vertical bearing. This may be attributed to the empiricism of calibrated factors in the method, specifically unbounded confinement effect and the simplifications implicitly applied in the method based on the aforementioned discussion. There does not appear to be a significant trend in these results with respect to the embedment depth d_{embed}/d_{col}.
- The proposed model predicts the experimentally observed moment strengths with reasonable accuracy. On average, the test-to-predicted ratio $M_{max}^{test}/M_{max}^{Model}$ = 0.99 with a CoV = 0.13 across all the test specimens, indicating significantly improved performance over the SDM approach. Additionally, the method represents the effects associated with each of the three scenarios outlined previously. Specifically, the approach results in the following average test-to-predicted ratios: (1) Scenario 1—breakout of concrete failure cone in the absence of attached horizontal reinforcement—that is, for the Tests 1G–5G, the average $M_{max}^{test}/M_{max}^{Model}$ = 1.05, with a CoV of 0.13; (2) Scenario 2—breakout of concrete failure cone in the presence of attached horizontal reinforcement—that is, for the Tests 1–3, the average $M_{max}^{test}/M_{max}^{Model}$ = 0.92, with a CoV of 0.14; and (3) Scenario 3—shear failure of concrete in the presence of horizontal reinforcement and vertical stirrups—that is, for the Tests 4 and 5, the average $M_{max}^{test}/M_{max}^{Model}$ = 0.96, with a CoV of 0.08. Thus, the proposed method appears to provide excellent estimates of test response over the subsets of tests (corresponding to each scenario), indicating that it represents the physics and internal stress distributions. Moreover, there is no significant trend in this accuracy with respect to any of the test variables, including the embedment depth, d_{embed}/d_{col} as illustrated in Figure 11(b).

As per the proposed model, the connection strength, M_{max}^{Model}, is attained after significant inelastic deformation and damage have occurred. As a result, this may not be suitable for the design of the base connection (especially if a strong-base–weak-column design is followed as per current practice). A fraction of the ultimate strength could be used for design purposes. This fraction may be taken between

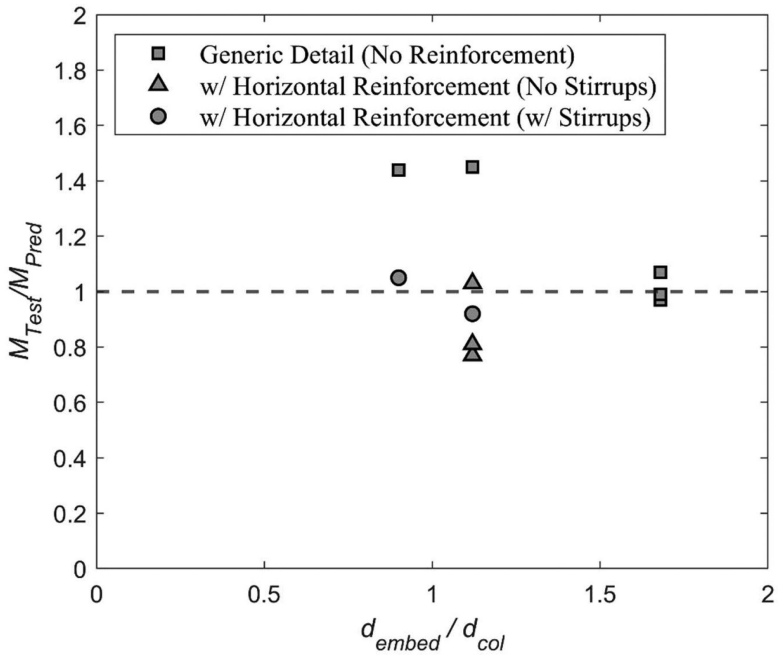

(a) AISC Seismic Design Manual *method*

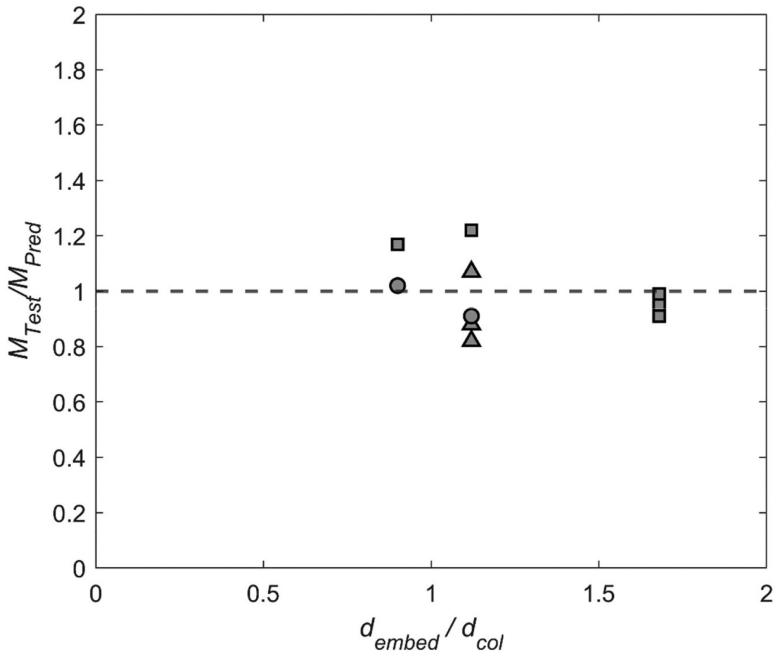

(b) Proposed model

Fig. 11. Test-predicted ratios for all experiments from AISC SDM method and the proposed model plotted against d_{embed}/d_{col}.

0.7–0.8, which represents the ratio between the yield and ultimate moment as observed in tested specimens in this program as well as in Grilli et al. (2017).

SUMMARY AND CONCLUSIONS

Embedded column base (ECB) connections are widely used in mid- to high-rise steel moment frames to resist base moments. Despite their prevalence, methods available to design and estimate their strength rely on approaches originally developed for components such as steel coupling beams embedded in concrete shear walls or composite beam column connections that are similar to ECB connections. While similar in some aspects, these components have significant differences from ECB connections that limit their applicability and accuracy. This study presents findings from five tests representative of ECB connections in the United States. These connections include horizontal reinforcement attached to the column flanges and complement previous experiments (conducted by Grilli et al., 2017) that did not include such reinforcement. Two techniques of attaching the reinforcement were examined, including reinforcement bars welded directly to the column flange or U-bar hairpins wrapped around the column. The tests from this study were considered collectively in developing behavioral insights, evaluating the existing strength characterization approaches, and proposing a new one.

The main observation was that while the attachment of horizontal reinforcement increases moment strength due to the development of horizontal forces, it produces a tension field behind the column. This reduces the restraint the concrete provides to base plate uplift, in turn decreasing moment strength due to vertical bearing stresses. For the specimens tested in this study, the decrease in moment strength (due to vertical stresses) is greater than the increase in moment strength (due to the horizontal stresses), such that the net effect is detrimental. Introduction of vertical reinforcement in the form of stirrups mitigates this problem to an extent by changing the failure mode to shear-friction along a nearly vertical plane rather than concrete breakout. On the other hand, the attachment of horizontal reinforcement significantly increases the rotational ductility of the connections (in the range of 0.06 rad) with respect to details without such reinforcement (in the range of 0.035 rad). These factors may influence detail selection in different contexts—for example, seismic versus nonseismic.

A strength model is proposed to represent these various failure mechanisms. For the horizontal bearing mechanism, the model relies on a stress-block based approach similar to that outlined by Grilli and Kanvinde (2017). For the vertical bearing mechanism, the model considers three scenarios for concrete breakout on the tension side of the connection, depending on the type of reinforcement used, and appears to provide uniformly accurate strength predictions across the different tested configurations and test programs. These predictions are superior compared to the current approach adopted in the AISC *Seismic Design Manual*. From a design standpoint, the use of this model is likely to reduce conservatisms of the AISC SDM model, while providing adequate safety.

Despite the accuracy of the proposed approach and the improvement (with knowledge advancement) over the current approaches for strength characterization and design of ECB connections, the model has numerous limitations. The model is only validated against 10 tests because these are the only available data on ECB connections. The proposed method considered different failure modes pertaining to the uplift/vertical resistance; however, other limit states associated with vertical bearing are also possible depending on the connection configuration, including (1) concrete breakout under the compression toe of the lower base plate (due to placement of the column on a thin layer of concrete) or (2) yielding of the base plate if not sufficiently thick. These may be resolved by using the internal force transfer mechanisms outlined in this study, albeit with consideration of force capacities associated with these other limit states; additional testing and calibration may be required for this purpose. Additionally, it is noted that the flexural deformations of the column may result in separation between the column flanges and footing (especially if no horizontal reinforcement is provided—as noted by Grilli and Kanvinde, 2017). Under such conditions, the axial compression may not be effectively transferred to the footing through the face-bearing plates on the top of the footing. This may result in punching failure of the supporting slab under the embedded base plate if it is not adequately designed. This failure state was not possible in the test setup of this study. Finally, the approach presented here does not include a reliability study to estimate or recommend ϕ factors. If the approach is used as is, then ϕ implicitly equals 1.0; this is similar to the current approach in the AISC *Seismic Design Manual* (2018).

In conclusion, it is emphasized that the response of these connections is controlled by nonlinear interactions between the various components (steel column/base, concrete, and reinforcement). As a result, it is challenging to develop a design method that explicitly satisfies equilibrium, compatibility, and nonlinear constitutive response of the various components, while also being convenient to apply in a professional setting. Consequently, the method presented in this study is based on some simplifying assumptions. This implies that caution should be exercised in extrapolating the results of this study to details that are highly dissimilar from those examined in this study.

ACKNOWLEDGMENTS

The authors are grateful to the American Institute of Steel Construction and the Charles Pankow Foundation for providing major funding for this project. The authors thank the advisory committee of the project: Mason Walters, Geoff Bomba, and Ali Roufegarinejad of Forell/Elsesser Engineers; Jim Malley of Degenkolb Engineers; Chia-Ming Uang of the University of California at San Diego; Subhash Goel of the University of Michigan; Tom Sabol of Engelkirk Structural Engineers; Tim Fraser of Structural Steel Detailing; Tom Kuznick of Herrick Steel; Joe Zona of Simpson Gumpertz and Heger; Rick Drake of Fluor Corporation; and Devin Huber of AISC.

REFERENCES

ACI (2019), *Building Code Requirements for Structural Concrete and Commentary*, ACI 318-19, Farmington Hills, Mich.

AISC (2016), *Seismic Provisions for Structural Steel Buildings* ANSI/AISC 341-16, American Institute of Steel Construction, Chicago, Ill.

AISC (2018), *Seismic Design Manual*, 3rd Ed., American Institute of Steel Construction, Chicago, Ill.

Anderson, N.S. and Meinheit, D.F. (2005), "Pryout Capacity of Cast-In Headed Stud Anchors," *PCI Journal*, Vol. 50, No. 2, pp. 90–112.

ASCE (1994), "Guidelines for Design of Joints between Steel Beams and Reinforced Concrete Columns," ASCE Task Committee on Design Criteria for Composite Structures in Steel and Concrete, *Journal of Structural Engineering*, ASCE, Vol. 120, No. 8, pp. 2,330–2,357.

Astaneh, A., Bergsma, G., and Shen, J.H. (1992), "Behavior and Design of Base Plates for Gravity, Wind and Seismic Loads," *Proceedings of the National Steel Construction Conference*, AISC, Chicago, Ill.

Cui, Y., Nagae, T., and Nakashima, M. (2009), "Hysteretic Behavior and Strength Capacity of Shallowly Embedded Steel Column Bases," *Journal of Structural Engineering*, ASCE, Vol. 135, No. 10, pp. 1,231–1,238. https://doi.org/10.1061/(ASCE)ST.1943 -541X.0000056

Fahmy, M., Stojadinovic, B., and Goel, S.C. (1999), "Analytical and Experimental Behavior of Steel Column Bases," *Proceedings of the 8th Canadian Conference on Earthquake Engineering*, Canadian Association for Earthquake Engineering, Ottawa.

Falborski, T., Torres-Rodas, P., Zareian, F., and Kanvinde, A. (2020), "Effect of Base-Connection Strength and Ductility on the Seismic Performance of Steel Moment-Resisting Frames," *Journal of Structural Engineering*, ASCE, Vol. 146, No. 5.

FIB (1990), *Model Code*, Comité Euro-International du Beton, Lausanne, Switzerland.

Fisher, J.M. and Kloiber, L.A. (2006), *Base Plate and Anchor Rod Design*, Design Guide 1, 2nd Ed., AISC, Chicago, Ill.

Fuchs, W., Eligehausen, R., and Breen, J.E. (1995), "Concrete Capacity Design (CCD) Approach for Fastening to Concrete," *ACI Structural Journal*, Vol. 92, No. 1, pp. 73–94.

Gomez, I., Deierlein, G., and Kanvinde, A. (2010), "Exposed Column Base Connections Subjected to Axial Compression and Flexure," Final Report, AISC, Chicago, Ill.

Grilli, D., Jones, R., and Kanvinde, A. (2017), "Seismic Performance of Embedded Column Base Connections Subjected to Axial and Lateral Loads," *Journal of Structural Engineering*, ASCE, Vol. 143, No. 5. 04017010. https://doi.org/10.1061/(ASCE)ST.1943-541X.0001741

Grilli, D.A. and Kanvinde, A. (2017), "Embedded Column Base Connections Subjected to Seismic Loads: Strength Model," *Journal of Constructional Steel Research,* Vol. 129, pp. 240–249.

Hanks, K.N. and Richards, A. (2019), "Experimental Performance of Block-Out Connections at the Base of Steel Moment Frames," *Journal of Structural Engineering*, ASCE, Vol. 145, No. 7, 04019057. https://doi.org/10.1061/(ASCE)ST.1943-541X .0002333

Harris, K.A., Mitchell, D., Cook, W.D., and Redwood, R.G. (1993), "Seismic Response of Steel Beams Coupling Reinforced Concrete Walls," *Journal of the Structural Division*, pp. 3,611–3,629. 10.1061/(ASCE)0733-9445(1993)119:12(3611)

Hassan, A.S. (2022), "Seismic Performance of Dissipative, Biaxially Loaded and Embedded Column Base Connections," Doctoral Dissertation, Department of Civil and Environmental Engineering, University of California, Davis.

Hassan, A.S., Song, B., Galasso, C., and Kanvinde, A.M. (2022), "Seismic Performance of Exposed Column Base Plate Connections with Ductile Anchor Rods," *Journal of Structural Engineering*, ASCE. 10.1061/(ASCE)ST.1943-541X.0003298

Hetenyi, M. (1946), "Beams on Elastic Foundation: Theory with Applications in the Fields of Civil and Mechanical Engineering," University of Michigan Press.

Inamasu, H., de Castro e Sousa, A., Güell, G., and Lignos, D.G. (2021), "Anchor-Yield Exposed Column Bases for Minimizing Residual Deformations in Seismic-Resistant Steel Moment Frames," *Earthquake Engineering Structural Dynamics,* Vol. 50, No. 4, pp. 1,083–1,100. https://doi.org/10.1002/eqe.3392

Kanvinde, A.M., Higgins, P., Cooke, R.J., Perez, J., and Higgins, J. (2015), "Column Base Connections for Hollow Steel Sections: Seismic Performance and Strength Models," *Journal of Structural Engineering*, ASCE, Vol. 141, No. 7.

Krawinkler, H., Gupta, A., Medina, R., and Luco, N. (2000), "Loading Histories for Seismic Performance Testing of SMRF Components and Assemblies," Report No. SAC/BD-00/10, SAC Joint Venture, Richmond, Calif.

Marcakis, K. and Mitchell, D. (1980), "Precast Concrete Connections with Embedded Steel Members," *Prestressed Concrete Institute Journal*, Vol. 25, No. 4, pp. 88–116.

Mattock, A.H. and Gaafar, G.H. (1982), "Strength of Embedded Steel Sections as Brackets," *ACI Journal*, Vol. 79, No. 2, pp. 83–93.

Pertold, J., Xiao, R., and Wald, F. (2000a), "Embedded Steel Column Bases—I Experiments and Numerical Simulation," *Journal of Constructional Steel Research*, Vol. 56, No. 3, pp. 253–270.

Pertold, J., Xiao, R., and Wald, F. (2000b), "Embedded Steel Column Bases—II Design Model Proposal," *Journal of Constructional Steel Research*, Vol. 56, No. 3, pp. 271–286.

Richards, P.W., Barnwell, N.V., Tryon, J.E., and Sadler, A. (2018), "Flexural Strength and Stiffness of Block-Out Connections for Steel Columns," *Engineering Structures*, Vol. 173, pp. 404–415. https://doi.org/10.1016/j.engstruct.2018.06.055

SEAOC (2015), *2015 IBC SEAOC Structural/Seismic Design Manual Volume 1: Code Application Examples*, Sacramento, Calif.

Shahrooz, B.M., Remetter, M.E., and Qin, F. (1993), "Seismic Design and Performance of Composite Coupled Walls," *Journal of Structural Engineering,* ASCE, Vol. 119, No. 11, pp. 3,291–3,309.

Trautner, C.A., Hutchinson, T., Grosser, P.R., and Silva, J.F. (2017), "Investigation of Steel Column-Baseplate Connection Details Incorporating Ductile Anchors," *Journal of Structural Engineering*, ASCE, Vol. 143, No. 8, 04017074. https://doi.org/10.1061/(ASCE)ST.1943-541X.0001759

Vecchio, F.J. and Collins, M.P. (1986), "The Modified Compression-Field Theory for Reinforced Concrete Elements Subjected to Shear," *ACI Journal*, Vol. 83, No. 2, pp. 219–231.

Wald, F. (2000), "Column Base Modelling," in M. Ivanyi and C.C. Baniotopoulos, eds., *Semi-Rigid Joints in Structural Steelwork*, International Centre for Mechanical Sciences, Vol. 419, Springer, Vienna, pp. 227–288.